

Article

Waste Glass-Derived Tobermorite Carriers for Ag⁺ and Zn²⁺ Ions

Habib Rahman ¹, Qiu Li ²  and Nichola J. Coleman ^{1,*}

¹ School of Science, Faculty of Engineering and Science, University of Greenwich, Chatham Maritime, Kent ME4 4TB, UK; habib016@gmail.com

² State Key Laboratory of Silicate Materials for Architectures, Wuhan University of Technology, Wuhan 430070, China; qiu-li@whut.edu.cn

* Correspondence: n.coleman@gre.ac.uk; Tel.: +44-208-331-9825

Abstract: In this study, the layer-lattice calcium silicate hydrate mineral, tobermorite, was synthesized from waste green or amber container glass and separately ion-exchanged with Ag⁺ or Zn²⁺ ions under batch conditions. Hydrothermal treatment of stoichiometrically adjusted mixtures of waste glass and calcium oxide in 4 M NaOH_(aq) at 125 °C yielded tobermorite products of ~75% crystallinity with mean silicate chain lengths of 17 units after one week. Maximum uptake of Zn²⁺ ions, ~0.55 mmol g⁻¹, occurred after 72 h, and maximum uptake of Ag⁺ ions, ~0.59 mmol g⁻¹, was established within 6 h. No significant differences in structure or ion-exchange behavior were observed between the tobermorites derived from either green or amber glass. Composite membranes of the biopolymer, chitosan, incorporating the original or ion-exchanged tobermorite phases were prepared by solvent casting, and their antimicrobial activities against *S. aureus* and *E. coli* were evaluated using the Kirby–Bauer assay. *S. aureus* and *E. coli* formed biofilms on pure chitosan and chitosan surfaces blended with the original tobermorites, whereas the composites containing Zn²⁺-substituted tobermorites defended against bacterial colonization. Distinct, clear zones were observed around the composites containing Ag⁺-substituted tobermorites which arose from the migration of the labile Ag⁺ ions from the lattices. This research has indicated that waste glass-derived tobermorites are functional carriers for antimicrobial ions with potential applications as fillers in polymeric composites to defend against the proliferation and transmission of pathogenic bacteria.

Keywords: antimicrobial; chitosan; tobermorite; silver; zinc; ion-exchange; waste glass; recycling



Citation: Rahman, H.; Li, Q.; Coleman, N.J. Waste Glass-Derived Tobermorite Carriers for Ag⁺ and Zn²⁺ Ions. *J. Compos. Sci.* **2022**, *6*, 52. <https://doi.org/10.3390/jcs6020052>

Academic Editor:
Francesco Tornabene

Received: 20 January 2022
Accepted: 7 February 2022
Published: 9 February 2022

Publisher's Note: MDPI stays neutral with regard to jurisdictional claims in published maps and institutional affiliations.



Copyright: © 2022 by the authors. Licensee MDPI, Basel, Switzerland. This article is an open access article distributed under the terms and conditions of the Creative Commons Attribution (CC BY) license (<https://creativecommons.org/licenses/by/4.0/>).

1. Introduction

Despite the theoretical potential to recycle up to 90% of container glass, approximately 200 Mt of post-consumer soda-lime-silica glass is landfilled per annum [1]. The failure to effectively recycle container glass arises from various technical, geographical, and economic barriers, particularly compositional heterogeneity, wide dispersal coupled with poor collection infrastructure, inadequate separation from other wastes, and lack of regional demand [2–5].

Recent research to explore alternative options to upcycle waste container glass (also known as cullet) into value-added products includes the production of zeolites [2–4,6–10], silicate minerals [5,11–16], geopolymers [17–19], and ceramics [20–22] for applications in catalysis, sorption/separation technology, and construction. In this respect, several studies have utilized a facile one-pot hydrothermal method to synthesize the layer-lattice calcium silicate phase, 11Å tobermorite (Ca₅Si₆O₁₆(OH)₂·4H₂O), from a mixture of waste glass cullet and lime or other calcium-bearing wastes [2,5,11–14,23]. The waste glass-derived tobermorite products have demonstrated high cation exchange capacities for a range of heavy metal contaminants [5,11–13] and basic catalytic properties for organic condensation reactions [23].

In addition to their ion exchange and catalytic characteristics, synthetic tobermorites derived from analytical grade reagents are reported to be biocompatible with bone tissue [24]. They have been evaluated as therapeutic components in polymer composites for tissue regeneration and biomedical applications [25–27]. Furthermore, Ag⁺- and Zn²⁺-substituted tobermorites have been shown to exert antimicrobial activity against common Gram-positive (*Staphylococcus aureus*) and Gram-negative (*Pseudomonas aeruginosa* and *Escherichia coli*) bacteria [28,29].

Ag⁺- and Zn²⁺-bearing zeolites, clays, minerals, and nanoparticles have been incorporated into a wide range of polymer composites to confer antimicrobial properties on packaging, films, coatings, wound dressings, medical devices, and equipment [30–34]. Given this, it is considered that waste glass-derived tobermorites may be effective carriers of Ag⁺ and Zn²⁺ ions for incorporation into antimicrobial polymer composites.

In the present study, the hydrothermal synthesis of 11 Å tobermorite was attempted by processing waste green or amber container glass mixed with stoichiometric quantities of calcium oxide at 125 °C for 7 days in 1 or 4 M sodium hydroxide solution. The reaction products were characterized by powder X-ray diffraction analysis (XRD), Fourier transform infrared spectroscopy (FTIR), and ²⁹Si magic angle spinning nuclear magnetic resonance spectroscopy (MAS NMR). The tobermorite phases were ion-exchanged with Ag⁺ or Zn²⁺ ions from metal nitrate solutions under batch conditions. Composite films of chitosan and the original, Ag⁺- and Zn²⁺-substituted tobermorites were then prepared by solvent casting. An inhibition zone assay was used to determine their antimicrobial activity against *S. aureus* and *E. coli*.

2. Materials and Methods

2.1. Materials

Post-consumer green and amber bottles were collected from the municipal refuse in Rochester, Kent, UK, and all other analytical grade reagents were obtained from Sigma-Aldrich, Gillingham, UK. The bottles were rinsed in warm tap water to remove the paper labels and ground in a steel ball mill under dry conditions to pass 125 µm. Quantitative oxide analyses of the green and amber container glasses were obtained by X-ray fluorescence spectroscopy using a Bruker S2 PUMA Series 2 (Bruker AXS, Karlsruhe, Germany) and are listed in Table 1.

Table 1. Oxide compositions of waste green and amber container glass.

Oxide Component	Quantity in Green Cullet (wt%)	Quantity in Amber Cullet (wt%)
SiO ₂	72.15	70.82
Na ₂ O	13.21	13.75
CaO	10.48	10.03
Al ₂ O ₃	1.48	2.21
MgO	0.94	1.42
K ₂ O	0.59	0.87
Fe ₂ O ₃	0.46	0.43
SO ₃	0.28	0.31
Cr ₂ O ₃	0.27	0.04

2.2. Hydrothermal Synthesis and Characterization

Hydrothermal syntheses were carried out in duplicate by heating 3.5 g of ground green or amber glass, 1.5 g of calcium oxide, and 60 cm³ of 1 M or 4 M sodium hydroxide solution in PTFE-lined stainless steel autoclaves (Parr Instrument Company, Moline, IL, USA) at 125 °C for 7 days. Solid reaction products were separated by gravitational filtration, washed with deionized water to pH ~7, and dried to constant mass in air at 60 °C. Samples prepared from green glass in 1 M or 4 M sodium hydroxide solution were labeled ‘TG1’ and ‘TG4’, respectively, and similarly, those prepared from amber glass were labeled ‘TA1’ and ‘TA4’. The hydrothermal reaction products were characterized by powder XRD using

a Bruker D8 diffractometer (Bruker AXS, Karlsruhe, Germany), FTIR using a Perkin Elmer Spectrum Two spectrometer (Perkin Elmer, London, UK), and ^{29}Si MAS NMR using a JEOL JNM-ECX 300 MHz spectrometer (JEOL (UK) Ltd., Welwyn Garden City, UK) as described in [4]. 11 Å tobermorite, calcite and silver carbonate were identified from the powder XRD patterns using PDF files 01-074-2783, 01-071-3699 and 01-070-2184. A representative example of the phase identification of the experimental XRD data using the PDF files is given in Appendix A.

The notation used to describe the silicate structures of the tobermorite products is such that the symbol Q denotes one tetrahedral SiO_4^{4-} unit, and a superscript indicates the number of other Q units to which it is bonded. Substitution by an AlO_4^{5-} unit is indicated in parentheses; for example, a mid-chain SiO_4^{4-} unit bonded between one SiO_4^{4-} unit and one AlO_4^{5-} unit is represented as $\text{Q}^2(1\text{Al})$. The tobermorite yield was estimated from the ^{29}Si MAS NMR spectra using the following relationship:

$$\text{Tobermorite yield} = [(\Sigma\text{Q}^n - \Sigma\text{Q}^4) \times 100] / \Sigma\text{Q}^n \quad (1)$$

where ΣQ^n is the sum of the intensities of all silicate resonances.

2.3. Ag^+ and Zn^{2+} Ion-Exchange

Prior to ion-exchange, TG4 and TA4 were lightly ground by mortar and pestle to pass 125 μm . The Ag^+ - and Zn^{2+} -substituted tobermorites were prepared by contacting 1.50 g of TG4 or TA4 with 200 cm^3 of 0.5 mM silver or zinc nitrate solution for 5 days at 25 °C (in a dark room to minimize the reduction of the silver cations). Then, 0.5 cm^3 aliquots of the supernatant solution were withdrawn at 1, 3, 6, 24, 48, 72, and 120 h for analysis by inductively coupled plasma optical emission spectroscopy (ICP-OES) using a TJA Iris simultaneous ICP-OES spectrometer (TJA, Waltham, MA, USA). After 5 days, the solid products were recovered by gravitational filtration, washed with 50 cm^3 of deionized water, and dried in air at 60 °C to constant mass prior to analysis by powder XRD and FTIR. The Ag^+ - and Zn^{2+} -substituted tobermorites derived from TG4 were labeled 'TG4-Ag' and 'TG4-Zn', and likewise, those prepared from TA4 were labeled 'TA4-Ag' and 'TA4-Zn'. All ion-exchange procedures were carried out in triplicate, and the relative standard deviations of the mean metal ion uptake data were less than 7% in all cases.

2.4. Preparation of Chitosan-Tobermorite Composite Films

Chitosan-tobermorite composite films were prepared at chitosan:tobermorite mass ratio of 5:1 by solvent casting. Chitosan solutions (2% (w/v)) were prepared in triplicate by dissolving 2.0 g of chitosan (molecular weight 50–190 kDa, degree of deacetylation 75–85%) in 100 cm^3 of 2% (v/v) ethanoic acid solution and stirring for 2 h at room temperature. Then, 0.40 g of tobermorite was added, and the mixtures were stirred for 5 h before casting 15 cm^3 aliquots onto polycarbonate plates (88 mm internal diameter) and drying in air at 60 °C to constant mass. Control membranes were prepared similarly in the absence of tobermorite. Composite films prepared with TG4, TG4-Ag, and TG4-Zn were labeled 'CTG4', 'CTG4-Ag', and 'CTG4-Zn', and those prepared with TA4, TA4-Ag and TA4-Zn were labeled 'CTA4', 'CTA4-Ag' and 'CTA4-Zn'.

2.5. Kirby-Bauer Inhibition Zone Assay

The antimicrobial properties of the chitosan-tobermorite composite films were assessed using the Kirby–Bauer inhibition zone method against *Staphylococcus aureus* NCIMB 9518 and *Escherichia coli* NCIMB 9132. Agar plates were inoculated by spreading with 0.2 cm^3 of overnight cultures of each bacterium. Three discs (10 mm diameter) of the chitosan-tobermorite films were placed on each spread plate. The plates were examined for clear zones after incubation at 37 °C for 24 h. Each assay was conducted in triplicate. The final population densities of the plates spread with *S. aureus* and *E. coli* were approximately 2×10^8 and 6×10^8 colony forming units per plate.

3. Results

3.1. Characterisation of Waste Container Glass-Derived Tobermorites

The powder XRD patterns of the amorphous green cullet and hydrothermal reaction products prepared in 1 M NaOH_(aq) (TG1) and 4 M NaOH_(aq) (TG4) are shown in Figure 1.

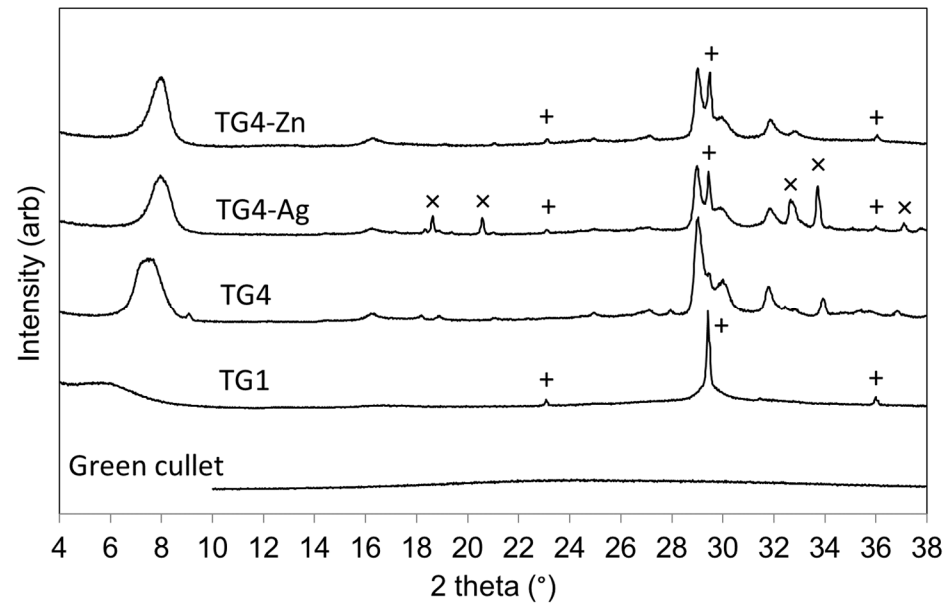


Figure 1. XRD patterns of green cullet and hydrothermal products of green cullet and calcium oxide in 1 M NaOH_(aq) (TG1) or 4 M NaOH_(aq) (TG4), and Ag⁺-exchanged TG4 (TG4-Ag) and Zn²⁺-exchanged TG4 (TG4-Zn). Key: + calcite; × silver carbonate; all other reflections arise from tobermorite.

These data indicate that the only crystalline product arising from the hydrothermal treatment of the green glass in 1 M NaOH_(aq) was calcite (CaCO₃). Conversely, increasing the alkalinity of the reaction medium to 4 M NaOH_(aq) gave rise to 11 Å tobermorite with a crystallinity of 74%. Similar results were obtained for the hydrothermal conditioning of amber glass (Figure 2), which yielded 75% crystalline 11 Å tobermorite in 4 M NaOH_(aq) and calcite in 1 M NaOH_(aq). The XRD patterns of TG4 and TA4 (Figures 1 and 2, respectively) closely resemble those of other bespoke and waste-derived tobermorites reported in the literature with broad (0 0 2) basal reflections arising from stacking defects along the *c*-axis [11–13,28,29].

FTIR spectra of the green and amber cullet and their hydrothermal reaction products are presented in Figure 3. The FTIR spectra of both glasses are characterized by a very broad band at approximately 1000 cm⁻¹ arising from various antisymmetric stretching modes of the amorphous Si-O-Si network and a less intense signal at ~770 cm⁻¹ originating from symmetric Si-O-Si stretching [35].

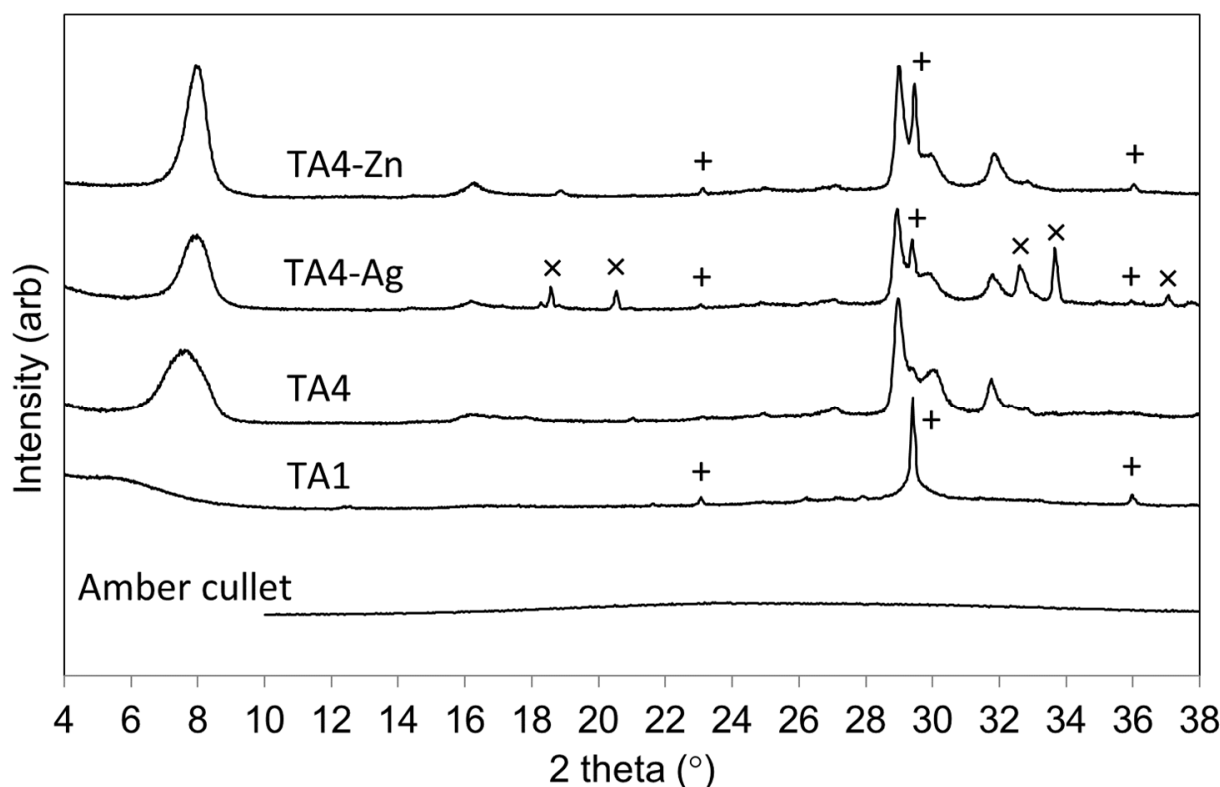


Figure 2. XRD patterns of amber cullet and hydrothermal products of amber cullet and calcium oxide in 1 M NaOH_(aq) (TA1) or 4 M NaOH_(aq) (TA4), and Ag⁺-exchanged TA4 (TA4-Ag) and Zn²⁺-exchanged TA4 (TA4-Zn). Key: + calcite; × silver carbonate; all other reflections arise from tobermorite.

Hydrothermal processing of green and amber glass in 1 M NaOH_(aq) resulted in a narrowing of the antisymmetric Si-O-Si stretching signal and a modest shift in maximum intensity to 970 cm⁻¹ (Figure 3). These changes indicate superior molecular ordering and a reduction in the degree of polymerization of the Qⁿ silicate species that are attributed to the formation of a calcium silicate hydrate gel precursor to tobermorite (Figure 3). As previously noted, these structural changes did not give rise to discrete XRD reflections for samples TG1 and TA1 (Figures 1 and 2, respectively).

The mid-chain Q² Si-O-Si stretching vibrations of the tobermorite lattices of the hydrothermal products, TG4 and TA4, are denoted by the intense sharp signal at 960 cm⁻¹, and the weaker band at ~800 cm⁻¹ is assigned to end-group Q¹ silicate stretching modes (Figure 3). Si-O-Si bending vibrations give rise to the signal at 670 cm⁻¹ [36].

Bending modes of water and hydroxyl groups are observed at 1640 cm⁻¹, and stretching modes of the carbonate ion of calcite appear at 1450 cm⁻¹ in the FTIR spectra of all hydrothermal products [23]. The appearance of calcite in the FTIR spectra, which may not be detectable by XRD, commonly arises from atmospheric carbonation during the hydrothermal preparation of tobermorites [36].

The deconvoluted ²⁹Si MAS NMR spectra of the hydrothermal products, TG4 and TA4, are shown in Figure 4 and the relative abundance of Qⁿ species, tobermorite-content, and mean chain length (MCL) of the silicate system of the tobermorite lattices are listed in Table 2. The ²⁹Si MAS NMR spectra of both TG4 and TA4 comprise signals arising from Q¹ chain-end and dimeric silicate species at -78 ppm, Q² and Q²(1Al) mid-chain tetrahedra at -84 and -80.5 ppm, respectively, and branching Q³(1Al) species at -92 ppm [37]. A very broad signal centered at approximately -108 ppm arises from amorphous silica comprising a predominance of Q⁴ species. The tobermorite-contents and silicate structures of the green and amber glass-derived hydrothermal products did not differ significantly (Table 2).

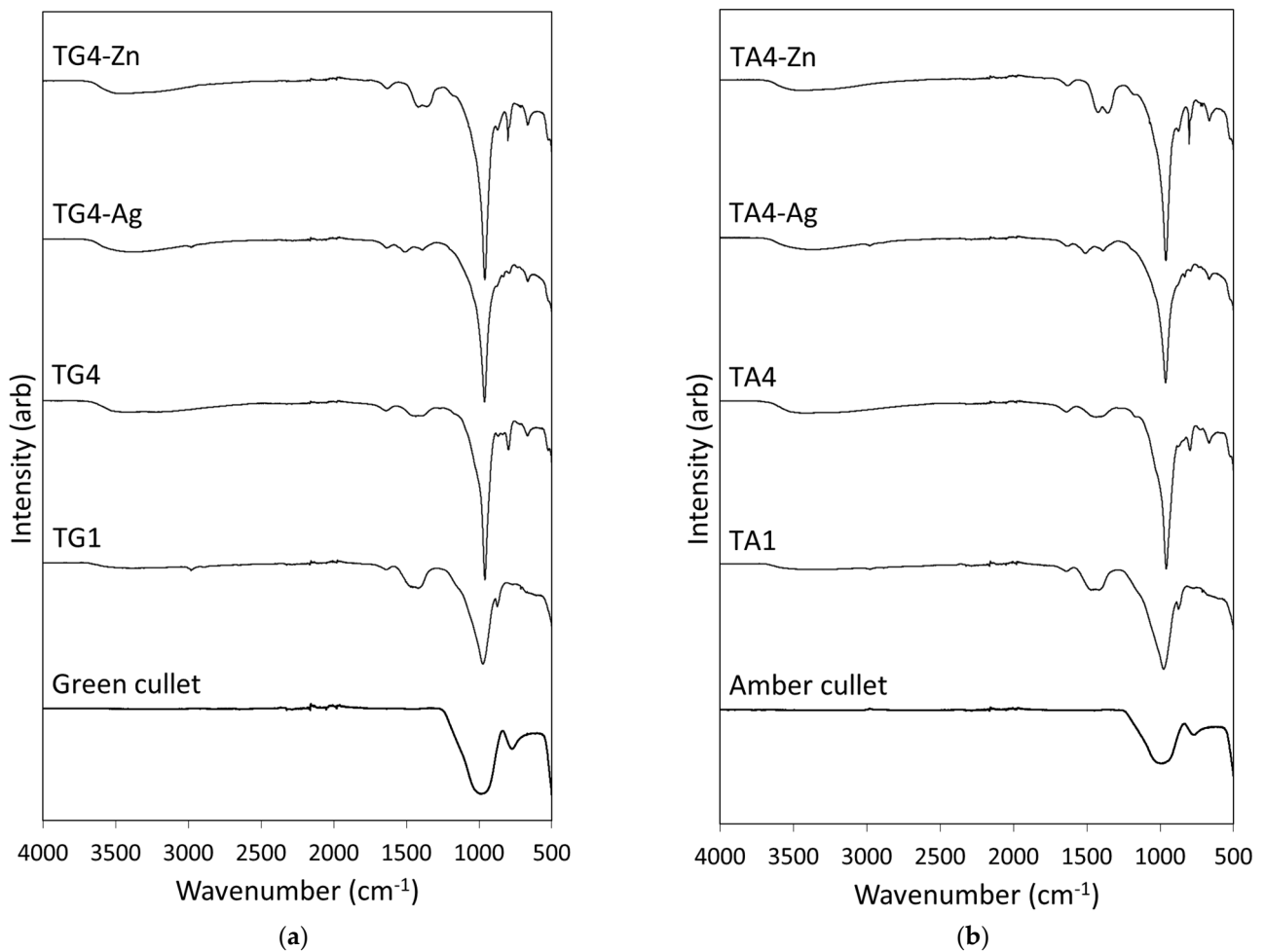


Figure 3. FTIR spectra of (a) green cullet and hydrothermal products of green cullet and calcium oxide in 1 M NaOH_(aq) (TG1) or 4 M NaOH_(aq) (TG4), and Ag⁺-exchanged TG4 (TG4-Ag) and Zn²⁺-exchanged TG4 (TG4-Zn); and FTIR spectra of (b) amber cullet and hydrothermal products of amber cullet and calcium oxide in 1 M NaOH_(aq) (TA1) or 4 M NaOH_(aq) (TA4), and Ag⁺-exchanged TA4 (TA4-Ag) and Zn²⁺-exchanged TA4 (TA4-Zn).

3.2. Ion-Exchange Properties of Waste Container Glass-Derived Tobermorites

The uptakes of Ag⁺ and Zn²⁺ ions from single metal nitrate solutions by TG4 and TA4 are plotted in Figure 5. Equilibrium Ag⁺-uptakes of $0.59 \pm 0.02 \text{ mmol g}^{-1}$ and $0.57 \pm 0.03 \text{ mmol g}^{-1}$ were established within 6 h for TG4 and TA4, respectively. Zn²⁺-uptake was observed to be considerably slower with maximum sorption of $0.53 \pm 0.02 \text{ mmol g}^{-1}$ (TG4) and $0.55 \pm 0.04 \text{ mmol g}^{-1}$ (TA4) at 120 h. There were no significant differences in the maximum uptakes of Ag⁺ and Zn²⁺ ions between the green or amber glass-derived tobermorite products.

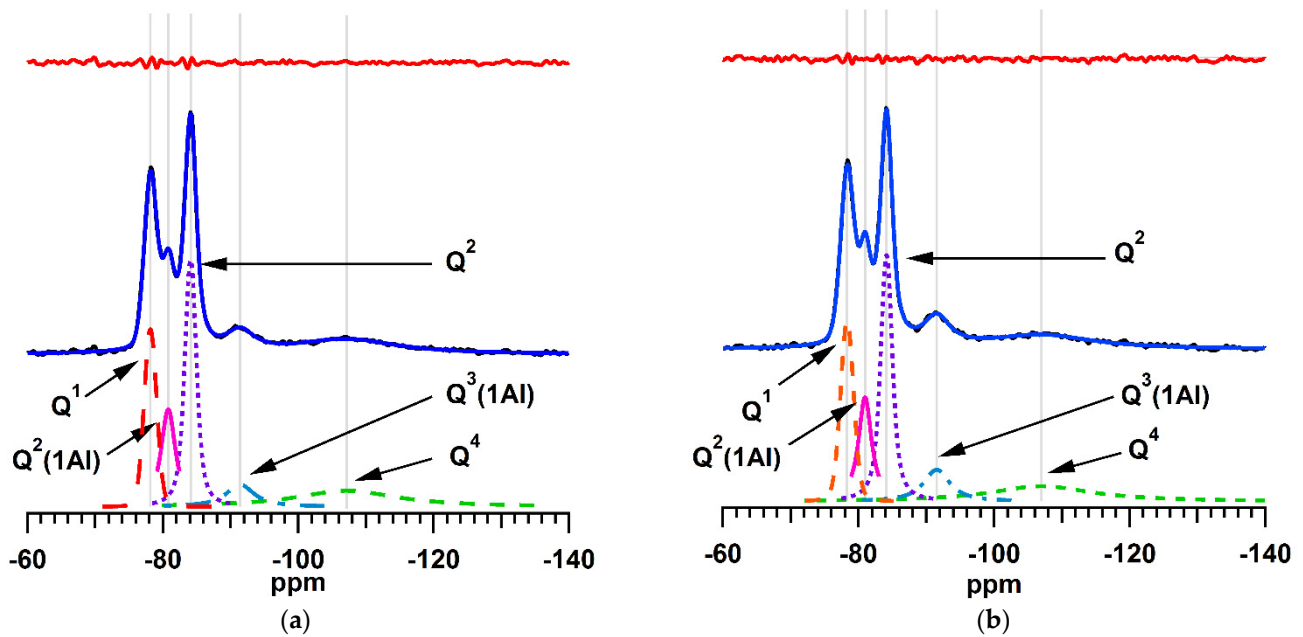


Figure 4. ^{29}Si MAS NMR spectra of (a) tobermorite product TG4 and (b) tobermorite product TA4. The calculated spectra are depicted as continuous royal blue lines superimposed over the experimental spectra (shown in black). The individually resolved resonances are presented as dashed lines. The residual between the calculated and experimental spectra is shown in red above the spectra.

Table 2. Structural properties of tobermorites derived from green (TG4) and amber (TA4) cullet.

Sample	Q ¹	Q ² (1Al)	Q ²	Q ³ (1Al)	Q ⁴	Tobermorite-Content	MCL
TG4	20.17	18.09	31.46	8.29	21.98	78 ± 4%	17.1
TA4	21.20	17.21	31.12	10.29	20.17	80 ± 4%	17.0

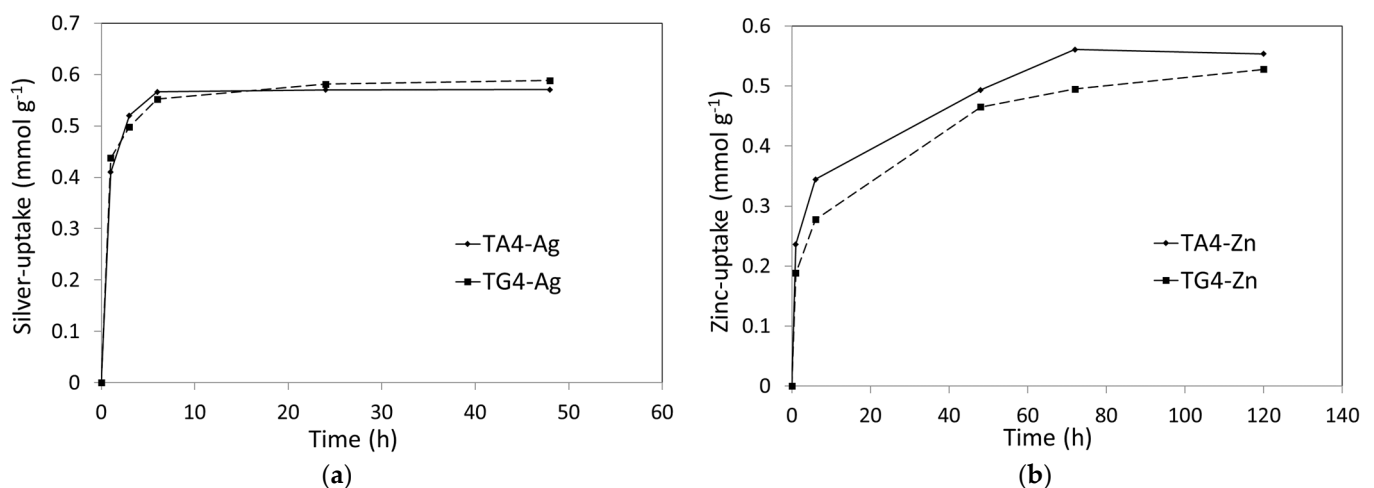


Figure 5. Uptakes of (a) Ag^+ ions and (b) Zn^{2+} ions by tobermorite products TG4 and TA4.

XRD analysis of the Ag^+ - and Zn^{2+} -loaded samples, TG4-Ag and TG4-Zn (Figure 1), and TA4-Ag and TA4-Zn (Figure 2), indicated that the integrity of the tobermorite structures was maintained after ion-exchange and that the incorporation of Ag^+ or Zn^{2+} ions did not cause disruption or amorphization of the lattices. In fact, the basal reflections of the tobermorites following ion exchange with Ag^+ or Zn^{2+} ions were narrower than those of

the original phases indicating that the uptake of these ions improved the stacking of the layers along the *c*-axis. Additional calcite was observed to form by atmospheric carbonation during the ion-exchange processes, and some silver carbonate was also precipitated during Ag^+ -exchange (Figures 2–4).

3.3. Antimicrobial Properties of Chitosan-Tobermorite Composites

Kirby-Bauer antibacterial inhibition zone tests using *S. aureus* and *E. coli* indicated that both microorganisms readily colonized the surfaces of the pure unblended chitosan control and the composite films prepared with the original TG4 and TA4 samples. Conversely, the composites containing Zn^{2+} -substituted tobermorites defended against bacterial biofilm formation, and distinct, clear zones also formed around the composites containing Ag^+ -substituted tobermorites (as shown in Figure 6). No significant difference was found between the extents of the clear zones around CTG4-Ag (1.8 ± 0.3 mm) and CTA4-Ag (1.7 ± 0.5 mm) exposed to *S. aureus*. Likewise, similarly-sized clear zones were observed around CTG4-Ag (0.8 ± 0.2 mm) and CTA4-Ag (0.7 ± 0.2 mm) incubated with *E. coli*. The defense of the surfaces of the Zn^{2+} -bearing composites against bacterial colonization with the absence of an extended clear zone indicates that the substituted Zn^{2+} ions were not readily released from the tobermorite lattice. In contrast, the clear zones around the Ag^+ -bearing composites are attributed to the migration of the labile Ag^+ ions into the surrounding medium.



Figure 6. Images of clear zones around discs (10 mm in diameter) of CTA-Ag in contact with (a) *E. coli* and (b) *S. aureus*.

4. Discussion

The landfilling and stockpiling of waste soda-lime-silica glass represent a significant failure in environmental sustainability. On average, approximately 5.8 MJ kg^{-1} of energy is required to produce new container glass, and the mining of raw materials gives rise to problematic erosion, flooding, land degradation, and pollution [38–40]. Accordingly, alternative upcycling of unwanted post-consumer container glass into functional value-added materials has been explored in many recent studies [3–19].

The present study confirms that soda-lime-silica container glass, irrespective of color, represents a suitably reactive and consistent feedstock for the facile hydrothermal synthesis of 11 \AA tobermorite. The processing of either green or amber glass with a stoichiometric addition of calcium oxide at $125 \text{ }^\circ\text{C}$ in $4 \text{ M NaOH}_{(\text{aq})}$ generated a high yield ($\sim 80\%$) of crystalline ($\sim 75\%$) tobermorite within 1 week. The yields, degrees of crystallinity, and structures of these container glass-derived tobermorites compare well with those of tobermorites synthesized from analytical grade reagents [25,28,29]. A reaction medium of $1 \text{ M NaOH}_{(\text{aq})}$ was found to be insufficiently alkaline to produce crystalline tobermorite within 7 days. However, a calcium silicate gel precursor appears to have formed under these conditions.

The use of natural and synthetic zeolites, clays, and silicate frameworks as carriers for antimicrobial Ag^+ and Zn^{2+} ions has received increasing attention in the quest to control the transmission of pathogenic microorganisms [28,30,31,41–48]. Silver ions are soft acids that target DNA and disrupt the chemistry of microbial metalloproteins involved in respiration, membrane structure, replication, and metabolism, by binding with thiol groups [49]. By virtue of their myriad antimicrobial mechanisms, silver ions are very broad spectrum, with over

600 susceptible pathogenic strains. Zinc ions possess less extensive antimicrobial properties, which arise from their interference in proton transfer processes and nutrient uptake.

The uptakes of Ag^+ and Zn^{2+} ions by the container glass-derived tobermorites in the present study are compared with those of other natural and synthetic silicate-based carriers reported in the recent literature in Table 3 [28,30,31,41–48]. The uptakes of Ag^+ ions by the green and amber glass-derived tobermorites are within the reported range for zeolite Y [44,45] and greater than those of analcime [41], chabazite [31], and montmorillonite [48]. However, the extents of Ag^+ -loading of TG4 and TA4 are inferior to those of zeolites A [30,32] and X [43], ZSM-5 [45], clinoptilolite [47], and the titanosilicate frameworks JDF-L1 and AM-4 [46]. Zn^{2+} -uptakes by TG4 and TA4 are comparable with that of titanosilicate AM-4 [46], superior to those of analcime [41], ZSM-5 [45], JDF-L1 [46], chabazite [31], clinoptilolite [47] and montmorillonite [48], and inferior to those of zeolites A [30,42], X [43] and Y [44,45].

Table 3. Uptake of Ag^+ and Zn^{2+} ions by various silicate lattice and framework phases.

Mineral Phase	Ag^+ -Uptake(mmol g^{-1})	Zn^{2+} -Uptake(mmol g^{-1})
Glass-derived tobermorite (this study)	0.57–0.59	0.53–0.55
Sodium metasilicate-derived tobermorite [28]	0.96	2.26
Synthetic analcime [41]	0.30	0.028
Zeolite A [42]	3.55	1.52
Zeolite A [30]	1.22	2.81
Zeolite X [43]	3.95	2.77
Zeolite Y [44]	0.046–0.73	0.83
Zeolite Y [45]	3.13	1.19
Zeolite ZSM-5 [45]	1.11	0.32
Titanosilicate JDF-L1 [46]	0.82	0.16
Titanosilicate AM-4 [46]	1.33	0.57
Natural chabazite [31]	0.12	0.018
Clinoptilolite [47]	1.23	0.22
Montmorillonite [48]	0.24	0.29

The more rapidly established steady-state uptake of Ag^+ ions (6 h) compared with that of Zn^{2+} ions (≥ 72 h) is attributed to the superior mobility of the Ag^+ ions within the tobermorite lattice arising from their inferior charge density and lower degree of hydration. Monovalent cations are known to substitute exclusively for the labile interlayer cations in tobermorite, whereas divalent cations can also replace Ca^{2+} ions from the structural layers [28]. Some isomorphic exchange of Zn^{2+} for structural Ca^{2+} ions is also likely to account for the comparatively long equilibrium times for the uptake of Zn^{2+} ions observed in this study.

The extents of Ag^+ - and Zn^{2+} -substitution of the container glass-derived tobermorites in the present study are lower than those reported for synthetic tobermorite derived from analytical grade sodium metasilicate and calcium oxide in 4 M $\text{NaOH}_{(\text{aq})}$ at 100 °C for 19 days [28]. Ongoing work to improve the ion-exchange properties of the green and amber glass-derived tobermorite products is now underway by optimizing the hydrothermal reaction parameters (i.e., alkalinity, temperature, reaction time, solid:solution ratio) and adjusting the reagent stoichiometry. For example, the substitution of up to 15% Si^{4+} for Al^{3+} within the tobermorite lattice is known to improve cation exchange capacity. A range of industrial Al-bearing waste streams is currently being considered additional feedstock for aluminum.

S. aureus is a Gram-positive facultative anaerobe commensal within the human microbiome and a principal opportunistic pathogen in skin and respiratory tract infections [50]. *E. coli* is a Gram-negative facultative anaerobe that produces vitamin K_2 in the human gut. Pathogenic strains of *E. coli* are associated with various infections, including pneumonia and gastroenteritis. *S. aureus* and *E. coli* are both common nosocomial and foodborne

pathogens that can survive on inanimate surfaces for many months, thereby providing a continuous transmission source in hospitals and food outlets via transiently contaminated hands [51]. One strategy to defend against the spread of such pathogens is the use of reactive antimicrobial surfaces in hospitals and for the processing, preparation, and storage of food [30–34,52]. As previously mentioned, a range of Ag⁺- and Zn²⁺-bearing zeolites, clays, minerals, and nanoparticles have been incorporated into polymer composites to confer antimicrobial properties on medical devices, films, coatings, and packaging [30–34,52].

In the present study, composite films of the biopolymer chitosan and Ag⁺- or Zn²⁺-substituted glass-derived tobermorites successfully defended against biofilm formation by *S. aureus* and *E. coli*. The large soft Ag⁺ ions of low charge-density were reversibly retained within the ion-exchangeable layers of the tobermorite lattice and subsequently migrated into the surrounding media to create clear zones around the composite films exposed to both bacteria (Table 3, Figure 6). Conversely, the smaller, more highly charge-dense Zn²⁺ ions did not generate distinct, clear zones beyond the perimeters of the films. The apparent retention of the exchanged Zn²⁺ ions is attributed to their superior electrostatic attraction to the negatively charged tobermorite lattice. It may also have arisen from complexation with structural oxygen and hydroxyl groups.

The results obtained in the present study agree with those of other Ag⁺- and Zn²⁺-bearing zeolites and clays that report inferior metal ion-release [43] and smaller or absent clear zones in *S. aureus* and *E. coli* Kirby–Bauer assays for Zn²⁺ relative to Ag⁺ [30,43,44]. Although, conversely, one study observed similar zones of inhibition in a culture of *S. aureus* for montmorillonite clay loaded with either 0.24 mmol g⁻¹ Ag⁺ or 0.29 mmol g⁻¹ Zn²⁺ [46].

As stated, ongoing research now concerns the optimization of the Ag⁺- and Zn²⁺-exchange characteristics of container glass-derived tobermorites to enable a more comprehensive appraisal of their potential as carriers in reactive antimicrobial composites. Further work to evaluate the maximum uptakes and subsequent release profiles of single and binary combinations of antimicrobial metal ions such as Ag⁺, Zn²⁺, and Cu²⁺ by the glass derived-tobermorites is now warranted, along with estimations of their minimum inhibitory and minimum bactericidal concentrations against a range of problematic microorganisms. In addition, the antimicrobial, physicochemical and mechanical properties of selected sustainable biopolymer-tobermorite composites will be explored.

5. Conclusions

This study has confirmed that soda-lime-silica container glass is a suitable feedstock for the facile and reproducible hydrothermal synthesis of 11 Å tobermorite, irrespective of color. The extents of Ag⁺- and Zn²⁺-uptake by green and amber glass-derived tobermorite products were found to be in the middle of the ranges reported for those of other zeolites, clays, and silicate framework materials. Composite films of chitosan and Ag⁺- or Zn²⁺-substituted glass-derived tobermorites defended against surface colonization and biofilm formation by *S. aureus* and *E. coli*. The migration of labile Ag⁺ ions from the tobermorite lattice created clear zones around the composite films, whereas the Zn²⁺ ions did not. Optimization of the hydrothermal treatment of the container glass offers the potential to improve the ion-exchange capacities of the tobermorite products.

Author Contributions: Conceptualization, N.J.C.; methodology, N.J.C.; software, N.J.C. and Q.L.; validation, N.J.C., H.R., and Q.L.; formal analysis, N.J.C., H.R., and Q.L.; investigation, H.R. and N.J.C.; resources, N.J.C.; data curation, N.J.C.; writing—original draft preparation, N.J.C.; writing—review and editing, H.R. and Q.L.; visualization, N.J.C.; supervision, N.J.C.; project administration, N.J.C.; funding acquisition, N.J.C. All authors have read and agreed to the published version of the manuscript.

Funding: This research received no external funding.

Institutional Review Board Statement: Not applicable.

Informed Consent Statement: Not applicable.

Data Availability Statement: The original data presented in this study are available on request from the corresponding author.

Conflicts of Interest: The authors declare no conflict of interest.

Appendix A

Example of XRD Phase Identification

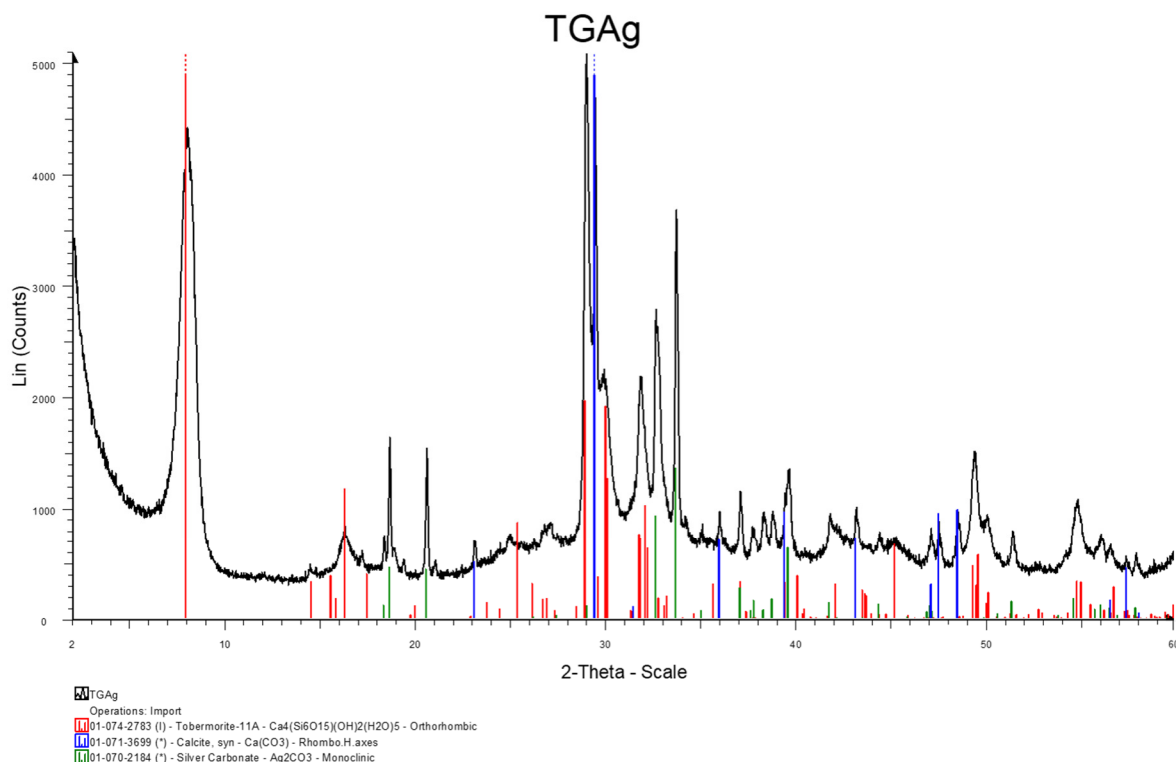


Figure A1. XRD pattern of TG4-Ag showing the identification of reflections from 11 Å tobermorite (PDF 01-074-2783, red lines), calcite (PDF 01-071-3699, blue lines) and silver carbonate (PDF 01-070-2184, green lines).

References

- Jiang, Y.; Ling, T.C.; Mo, K.H.; Shi, C. A critical review of waste glass powder—Multiple roles of utilization in cement-based materials and construction products. *J. Environ. Manag.* **2019**, *242*, 440–449. [[CrossRef](#)] [[PubMed](#)]
- Elmes, V.K.; Hurt, A.P.; Coleman, N.J. Mixed-phase ion-exchangers from waste amber container glass. *Materials* **2021**, *14*, 4887. [[CrossRef](#)] [[PubMed](#)]
- Taylor, J.H.; Elmes, V.E.; Hurt, A.P.; Coleman, N.J. Synthesis of feldspathoids and zeolite K–F from waste amber container glass. *Mater. Chem. Phys.* **2020**, *246*, 122805. [[CrossRef](#)]
- Maisuria, J.; Elmes, V.K.; Hurt, A.P.; Coleman, A.A.; Coleman, N.J. Hydrothermal synthesis of zeolites from green container glass. *Physicochem. Probl. Miner. Process.* **2020**, *56*, 784–796. [[CrossRef](#)]
- Malferrari, D.; Bernini, F.; Di Giuseppe, D.; Scognamiglio, V.; Gualtieri, A.F. Al-substituted tobermorites: An effective cation exchanger synthesized from “end-of-waste” materials. *ACS Omega* **2022**, in press. [[CrossRef](#)] [[PubMed](#)]
- Majdinasab, A.R.; Yuan, Q. Microwave synthesis of zeolites from waste glass cullet using indirect fusion and direct hydrothermal methods: A comparative study. *Ceram. Int.* **2019**, *45*, 2400–2410. [[CrossRef](#)]
- Majdinasab, A.R.; Manna, P.K.; Wroczynskyj, Y.; van Lierop, J.; Cicek, N.; Tranmer, G.K.; Yuan, Q. Cost-effective zeolite synthesis from waste glass cullet using energy efficient microwave radiation. *Mater. Chem. Phys.* **2019**, *221*, 272–287. [[CrossRef](#)]
- Terzano, R.; D’Alessandro, C.; Spagnuola, M.; Romagnoli, M.; Medici, L. Facile zeolite synthesis from municipal glass and aluminium solid wastes. *Clean-Soil Air Water* **2015**, *43*, 133–140. [[CrossRef](#)]
- Espejel-Ayala, F.; Chora Corella, R.; Morales Pérez, A.; Pérez-Hernández, R.; Ramírez-Zamora, R.M. Carbon dioxide capture utilizing zeolites synthesized with paper sludge and scrap-glass. *Waste Manag. Res.* **2014**, *32*, 1219–1226. [[CrossRef](#)] [[PubMed](#)]
- Lin, C.; Wang, D.; Ye, S. Synthesis of micro-mesoporous glass-analcime composite structure with soda-lime-silica glass as raw material. *Funct. Mater. Lett.* **2019**, *12*, 1950021. [[CrossRef](#)]

11. Coleman, N.J. 11 Å tobermorite ion exchanger from recycled container glass. *Int. J. Environ. Waste Manag.* **2011**, *8*, 366–382. [[CrossRef](#)]
12. Coleman, N.J.; Li, Q.; Raza, A. Synthesis, structure and performance of calcium silicate ion exchangers from recycled container glass. *Physicochem. Probl. Miner. Process.* **2014**, *50*, 5–16. [[CrossRef](#)]
13. Coleman, N.J.; Trice, C.J.; Nicholson, J.W. 11 Å tobermorite from cement bypass dust and waste container glass: A feasibility study. *Int. J. Miner. Process.* **2009**, *93*, 73–78. [[CrossRef](#)]
14. Majdinasab, A.; Yuan, Q. Synthesis of Al-substituted 11Å tobermorite using waste glass cullet: A study on the microstructure. *Mater. Chem. Phys.* **2020**, *250*, 123069. [[CrossRef](#)]
15. Elmes, V.E.; Mendham, A.P.; Coleman, N.J. A waste-derived lithium metasilicate basic catalyst. In Proceedings of the 2017 2nd International Conference on Materials Science and Nanotechnology (ICMSNT 2017), Auckland, New Zealand, 19–22 April 2017; Volume 109, p. 03004. [[CrossRef](#)]
16. Coleman, N.J.; Hurt, A.P.; Raza, A. Hydrothermal synthesis of lithium silicate from waste glass. A preliminary study. *Physicochem. Probl. Miner. Process.* **2015**, *51*, 685–694. [[CrossRef](#)]
17. Medina, T.J.; Arredondo, S.P.; Corral, R.; Jacobo, A.; Zárraga, R.A.; Rosas, C.A.; Cabrera, F.G.; Bernal, J.M. Microstructure and Pb²⁺ adsorption properties of blast furnace slag and fly ash based geopolymers. *Minerals* **2020**, *10*, 808. [[CrossRef](#)]
18. Bobirić, C.; Shim, J.-H.; Park, J.-Y. Leaching behavior of fly ash-waste glass and fly ash-slag-waste glass-based geopolymers. *Ceram. Int.* **2018**, *44*, 5886–5893. [[CrossRef](#)]
19. Zhang, Y.; Xiao, R.; Jiang, X.; Li, W.; Zhu, X.; Huang, B. Effect of particle size and curing temperature on mechanical and microstructural properties of waste glass-slag-based and waste glass-fly ash-based geopolymers. *J. Clean. Prod.* **2020**, *273*, 122970. [[CrossRef](#)]
20. Silva, R.V.; de Brito, J.; Lye, C.Q.; Dhir, R.K. The role of glass waste in the production of ceramic-based products and other applications: A review. *J. Clean. Prod.* **2017**, *167*, 346–364. [[CrossRef](#)]
21. Ayala Valderrama, D.M.; Gómez Cuaspid, J.A.; Roether, J.A.; Boccaccini, A.R. Development and characterization of glass-ceramics from combinations of slag, fly ash, and glass cullet without adding nucleating agents. *Materials* **2019**, *12*, 2032. [[CrossRef](#)] [[PubMed](#)]
22. Rambaldi, E. Pathway towards a high recycling content in traditional ceramics. *Ceramics* **2021**, *4*, 36. [[CrossRef](#)]
23. Elmes, V.K.; Edgar, B.N.; Mendham, A.P.; Coleman, N.J. Basic metallosilicate catalysts from waste green container glass. *Ceram. Int.* **2018**, *44*, 17069–17073. [[CrossRef](#)]
24. Maeda, H.; Tamura, T.; Kasuga, T. Improving the biocompatibility of tobermorite by incorporating calcium phosphate clusters. *Biomed. Mater. Eng.* **2017**, *28*, 31–36. [[CrossRef](#)] [[PubMed](#)]
25. Hurt, A.P.; Getti, G.; Coleman, N.J. Bioactivity and biocompatibility of a chitosan-tobermorite composite membrane for guided tissue regeneration. *Int. J. Biol. Macromol.* **2014**, *64*, 11–16. [[CrossRef](#)] [[PubMed](#)]
26. Hurt, A.P.; Kotha, A.K.; Trivedi, V.; Coleman, N.J. Bioactivity, biocompatibility and antimicrobial properties of a chitosan-mineral composite for periodontal tissue regeneration. *Polímeros* **2015**, *25*, 2015. [[CrossRef](#)]
27. Okuyama, T.; Maeda, H.; Ishida, E.H. Preparation of porous poly(L-lactic acid)/tobermorite composite membranes via electrospinning and heat treatment. *J. Mater. Sci.* **2012**, *47*, 643–648. [[CrossRef](#)]
28. Coleman, N.J.; Bishop, A.H.; Booth, S.E.; Nicholson, J.W. Ag⁺- and Zn²⁺-exchange kinetics and antimicrobial properties of 11 Å tobermorites. *J. Eur. Ceram. Soc.* **2009**, *29*, 1109–1117. [[CrossRef](#)]
29. Coleman, N.J. Aspects of the in vitro bioactivity and antimicrobial properties of Ag⁺- and Zn²⁺-exchanged 11 Å tobermorites. *J. Mater. Sci. Mater. Med.* **2009**, *20*, 1347–1355. [[CrossRef](#)]
30. Kaali, P.; Pérez-Madrigal, M.M.; Strömberg, E.; Aune, R.E.; Czél, G.; Karlsson, S. The influence of Ag⁺, Zn²⁺ and Cu²⁺ exchanged zeolite on antimicrobial and long term in vitro stability of medical grade polyether polyurethane. *EXPRESS Polym. Lett.* **2011**, *5*, 1028–1040. [[CrossRef](#)]
31. Torres-Giner, S.; Ana Torres, A.; Ferrándiz, M.; Fombuena, V.; Balart, R. Antimicrobial activity of metal cation-exchanged zeolites and their evaluation on injection-molded pieces of bio-based high-density polyethylene. *J. Food Saf.* **2017**, *37*, e12348. [[CrossRef](#)]
32. Predoi, D.; Iconaru, S.L.; Predoi, M.V. Fabrication of silver- and zinc-doped hydroxyapatite coatings for enhancing antimicrobial effect. *Coatings* **2020**, *10*, 905. [[CrossRef](#)]
33. Wattanawong, N.; Chatchaipaboon, K.; Sreekirin, N.; Aht-Ong, D. Migration, physical and antibacterial properties of silver zeolite/poly(butylene succinate) composite films for food packaging applications. *J. Reinf. Plast. Comp.* **2020**, *39*, 95–110. [[CrossRef](#)]
34. Quintero-Quiroz, C.; Botero, L.E.; Zárate-Triviño, D.; Acevedo-Yepes, N.; Saldarriaga Escobar, J.; Pérez, V.Z.; Javier Cruz Riano, L. Synthesis and characterization of a silver nanoparticle-containing polymer composite with antimicrobial abilities for application in prosthetic and orthotic devices. *Biomater. Res.* **2020**, *24*, 13. [[CrossRef](#)]
35. El Batal, H.A.; Hassan, M.Y.; Fanny, M.A.; Ibrahim, M.M. Optical and FT infrared absorption spectra of soda lime silicate glasses containing nano Fe₂O₃ and effects of gamma irradiation. *Silicon* **2017**, *9*, 511–517. [[CrossRef](#)]
36. Mostafa, N.Y.; Shaltout, A.A.; Omar, H.; Abo-El-Enein, S.A. Hydrothermal synthesis and characterization of aluminium and sulfate substituted 1.1 nm tobermorites. *J. Alloys Compd.* **2009**, *467*, 332–337. [[CrossRef](#)]
37. Houston, J.R.; Maxwell, R.S.; Carroll, S.A. Transformation of meta-stable calcium silicate hydrates to tobermorite: Reaction kinetics and molecular structure from XRD and NMR spectroscopy. *Geochem. Trans.* **2009**, *10*, 1. [[CrossRef](#)] [[PubMed](#)]

38. Conradt, R. Prospects and physical limits of processes and technologies in glass melting. *J. Asian Ceram. Soc.* **2019**, *7*, 377–396. [[CrossRef](#)]
39. Grbeš, A. A life cycle assessment of silica sand: Comparing the beneficiation processes. *Sustainability* **2016**, *8*, 11. [[CrossRef](#)]
40. Mishra, A. Impact of silica mining on environment. *J. Geogr. Reg. Plann.* **2015**, *8*, 150–156. [[CrossRef](#)]
41. Yousefpour, M. Modelling of adsorption of zinc and silver ions on analcime and modified analcime zeolites using central composite design. *Iran. J. Chem. Chem. Eng.* **2017**, *36*, 81–90. [[CrossRef](#)]
42. Benaliouche, F.; Hidous, N.; Guerza, M.; Zouad, Y.; Boucheffa, Y. Characterization and water adsorption properties of Ag- and Zn-exchanged A zeolites. *Microporous Mesoporous Mater.* **2015**, *209*, 184–188. [[CrossRef](#)]
43. Demirci, S.; Ustaoglu, Z.; Yilmazer, G.A.; Sahin, F.; Baç, N. Antimicrobial properties of zeolite-X and zeolite-A ion-exchanged with silver, copper, and zinc against a broad range of microorganisms. *Appl. Biochem. Biotechnol.* **2014**, *172*, 1652–1662. [[CrossRef](#)]
44. Peixoto, P.; Guedes, J.F.; Rombi, E.; Fonseca, A.M.; Aguiar, C.A.; Neves, I.C. Metal ion–zeolite materials against resistant bacteria, MRSA. *Ind. Eng. Chem. Res.* **2021**, *60*, 12883–12892. [[CrossRef](#)]
45. Abu Suleiman, L.; Haddadin, R.; Hodali, H.A. Antimicrobial activity of metal-loaded zeolites against “*S. aureus*” and “*E. coli*”. *Jordan J. Chem.* **2019**, *14*, 61–68.
46. Pérez-Carvajal, J.; Lalueza, P.; Casado, C.; Téllez, C.; Coronas, J. Layered titanosilicates JDF-L1 and AM-4 for biocide applications. *Appl. Clay Sci.* **2012**, *56*, 30–35. [[CrossRef](#)]
47. Top, A.; Ülkü, S. Silver, zinc, and copper exchange in a Na-clinoptilolite and resulting effect on antibacterial activity. *Appl. Clay Sci.* **2004**, *27*, 13–19. [[CrossRef](#)]
48. Özdemir, G.; Hoşgör-Limoncu, M.; Yapar, S. The antibacterial effect of heavy metal and cetylpridinium-exchanged montmorillonites. *Appl. Clay Sci.* **2010**, *48*, 319–323. [[CrossRef](#)]
49. Evans, A.; Kavanagh, K.A. Evaluation of metal-based antimicrobial compounds for the treatment of bacterial pathogens. *J. Med. Microbiol.* **2021**, *70*, 001363. [[CrossRef](#)]
50. Frickmann, H.; Hahn, A.; Berlec, S.; Ulrich, J.; Jansson, M.; Schwarz, N.G.; Warnke, P.; Podbielski, A. On the etiological relevance of *Escherichia coli* and *Staphylococcus aureus* in superficial and deep infections—A hypothesis-forming, retrospective assessment. *Eur. J. Microbiol. Immunol.* **2019**, *9*, 124–130. [[CrossRef](#)] [[PubMed](#)]
51. Kramer, A.; Schwebke, I.; Kampf, G. How long do nosocomial pathogens persist on inanimate surfaces? A systematic review. *BMC Infect. Dis.* **2006**, *6*, 130. [[CrossRef](#)] [[PubMed](#)]
52. Souza, V.G.L.; Pires, J.R.A.; Rodrigues, C.; Coelho, I.M.; Fernando, A.L. Chitosan composites in packaging industry—Current trends and future challenges. *Polymers* **2020**, *12*, 417. [[CrossRef](#)] [[PubMed](#)]